Computational Study of *p*-Xylene/*m*-Xylene Mixtures Adsorbed in NaY Zeolite

Véronique Lachet, Anne Boutin,* Bernard Tavitian,† and Alain H. Fuchs

Department of Physical Chemistry, Chimie-Physique des Matériaux Amorphes (URA 1104 CNRS), Bâtiment 490, Université de Paris-Sud, 91405 Orsay Cedex, France

Received: January 29, 1998

The properties of *p*-xylene and *m*-xylene adsorbed in sodium Y faujasite have been studied by grand canonical Monte Carlo simulation. Biased particle insertions and deletions were implemented to allow the computation of equilibrium adsorption isotherms of such complex molecules. Single species and binary mixtures isotherms at 423 K were calculated and compared to the available experimental data. Three binary mixtures corresponding to different gas phase compositions were studied. The *p*-xylene/*m*-xylene selectivities predicted from the simulation are in qualitative agreement with experiments: the zeolite NaY preferentially adsorbs the *m*-xylene isomer. A detailed analysis of the adsorbed phase structure reveals a unique adsorption site in the supercage of the zeolite located in front of the sodium cations in site II.

I. Introduction

The adsorption of aromatic molecules in zeolitic microporous materials is of great scientific interest in the context of separation and catalysis processes such as alkylation, transalkylation, and isomerization of *m*-xylene into *p*-xylene. For instance, the separation of *p*-xylene from C_8 aromatics (a mixture of xylene isomers and ethylbenzene molecules) is performed on the industrial scale using selective adsorption in synthetic faujasite type zeolite.[1] It is now known that the faujasite zeolite may be selective for one xylene isomer or another depending on the nature and the number of extraframework cations. However, the mechanism through which adsorption selectivity is generated is not yet understood.

A large number of microscopic and macroscopic measurements, such as crystallographic,[2−6] and IR,[6−8] studies, thermodynamic,[9−16] and diffusion coefficient,[17−21] measurements have been carried out on *p*-xylene/*m*-xylene mixtures adsorbed in faujasite zeolites. The works performed on Y zeolites with monovalent cations have revealed that both LiY[22] and NaY[14,15,22] are selective for *m*-xylene, while KY,[22−24] RbY,[22] and CsY[22] are selective for *p*-xylene. In a recent study of a barium-exchanged Y faujasite, Cottier et al.[14,15] have found that BaY is selective for *p*-xylene. In the case of X faujasites, the study of Allain et al.[25] shows that BaX is selective for *p*-xylene.

The need to gain a detailed insight into the behavior of zeolite/sorbate systems on the molecular scale has also inspired some molecular simulation studies, using molecular dynamics technique[26] and grand canonical[27] or canonical[28] Monte Carlo simulation. The grand canonical Monte Carlo (GCMC) simulation technique is well suited to adsorption studies: adsorption isotherms are obtained directly from the simulation by evaluating the average number of adsorbed molecules whose chemical potential equals that of the bulk gas at given temperature and pressure. As a first step toward the study of mixtures, it is possible to use adsorbed solution theories[29] (IAS) or statistical models (Ruthven et al.[16]) to predict the coadsorption isotherm from the single-component isotherms. In the case of *p*-xylene/*m*-xylene coadsorption in NaY and BaY faujasites, Cottier et al.[14] have failed to reproduce the experimental selectivities using the IAS theory because the adsorbed *p*-xylene/*m*-xylene mixture is not an ideal solution. The use of the statistical model of Ruthven et al.[16] gave very satisfactory results in the case of NaY; but in the case of BaY, the model predicted no selectivity whereas experiments have revealed a preferential adsorption of *p*-xylene.

An alternative to the calculation of the coadsorption selectivities would be to use Henry constants: from these zero coverage data, one can easily calculate the selectivity at zero loading. However, steric effects between adsorbed molecules can play an important role and can govern the selectivity at high loading. In the case of zeolite KY, for instance, no selectivity is observed for loadings up to two molecules per supercage; the preferential adsorption for *p*-xylene is only observed for coverage above two molecules per supercage. This is the reason why we have focused our attention on the high loading properties and GCMC adsorption isotherms rather than zero coverage data.

The exact coadsorption data at different coverages can be obtained directly from a GCMC simulation of a mixture in which the chemical potential of each component in the bulk phase is specified during the simulation. This direct coadsorption simulation has the advantage of giving information on the possible difference between the behavior of the single-component adsorbed phase and that of the multicomponent adsorbed phase. Such information can be very helpful in understanding molecular selectivity. To our knowledge, no work has been undertaken until now to investigate the adsorption properties of C_8 aromatic mixtures in faujasite-type zeolites by means of GCMC simulation. This is presumably due to the fact that the conventional GCMC simulation technique fails in predicting sorption equilibria in the case of complex adsorbates such as the xylene isomers. The present paper discusses our efforts to use biased GCMC algorithms for addressing these rather complex systems. Simulations have been performed at a temperature of 423 K to study the adsorption properties of *p*-xylene and *m*-xylene in the sodium Y faujasite (NaY). Single

* To whom correspondence should be addressed. E-mail: boutin@cpma.u-psud.fr. Fax: 33 1 69 15 42 00.

† Department of Applied Chemistry and Physical-Chemistry, Institut Français du Pétrole, 1 et 4 avenue de Bois Préau, BP 311, 92506 Rueil-Malmaison Cedex, France.

10.1021/jp980946j CCC: $15.00
Published on Web 10/27/1998

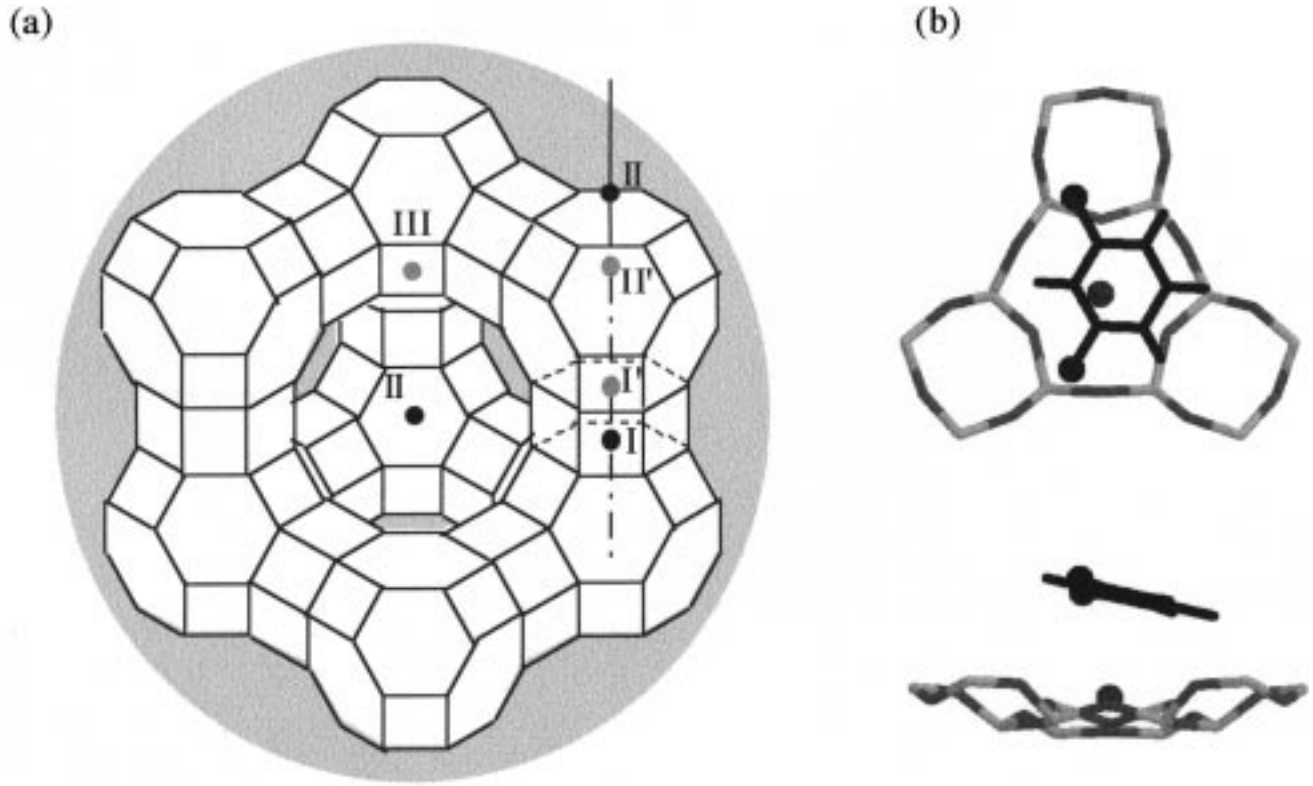

Figure 1. (a) Schematic view of a supercage of faujasite. The sites I for cations are located at the centers of the hexagonal prism, sites II are in front of the 6 T rings inside the supercage, and sites III are also in the supercage near the 4 T rings of sodalite cages. The T atoms are located at the vertexes of the cavity and the oxygen atoms occupy positions close to the centers of the lines. (b) Snapshot of a *m*-xylene molecule adsorbed in front of the six-ring near cation in site II in a NaY faujasite.

species and binary mixtures adsorption isotherms have been calculated and compared to the available experimental data. Three binary mixtures corresponding to different gas phase compositions have been studied. The predicted *p*-xylene/*m*-xylene selectivities from the simulation are in qualitative agreement with experiments. A detailed analysis of the adsorbed phase structure is presented.

II. Simulation Model

Structural Details. Zeolites are porous crystalline aluminosilicates. The framework consists of tetrahedral aluminum and silicon atoms bridged by oxygen atoms. The presence of aluminum atoms introduces charge defects which are compensated with some nonframework cations (sodium, potassium, barium, ...). The faujasite zeolites display cubic crystalline lattices. The microporous network is made of cuboctahedral sodalite cages with a diameter of about 6.5 Å. These cages are linked together in a tetrahedral arrangement by six oxygen atoms rings and form large cavities, named supercages. The supercages have a diameter of about 12.5 Å. They are interconnected in a tetrahedral arrangement by windows of diameter ~7.5 Å (Figure 1a). One cubic unit cell contains eight sodalite cages and eight supercages. The ratio of silicon to aluminum atoms and thus, the number of cations vary from one faujasite to another. A faujasite is named Y (or X) when it has a Si/Al ratio greater (or lower) than 1.5. A substantial number of diffraction studies have examined the location of extraframework cations in faujasite-type zeolites, including hydrated and dehydrated forms of zeolites X and Y.[30] However, in the case of monovalent cation forms of zeolite X, a significant proportion of cations are often undetected and the precise location of site III slightly differs from one author to another.[31]

Sodium cations in the NaY faujasite[2,32] are found to occupy mainly sites I (center of the hexagonal prism), I′ (in the sodalite cage at the center of the six-ring) and II (in the supercage near the six-ring of the sodalite cage) (see Figure 1a). In order to avoid introducing periodic crystal defects in the simulation model, we have chosen a full occupancy of sites I and II by sodium ions. This corresponds to a Si/Al ratio of 3, with 48 cations per unit cell. Distinction between Si and Al atoms leads to a heterogeneous distribution of Al atoms; thus, a unique average atom has been used in our model. The composition is thus $T_{192}O_{384}Na_{48}$, where T indicates tetrahedrally coordinated atoms (Si or Al). The framework structure of NaY is taken from neutron diffraction studies of Fitch et al.[2] The crystalline structure is described in the *Fd*3*m* space group. The cubic lattice parameter is 24.8536 Å.

One unit cell of zeolite (eight supercages) was used to construct the simulation box and periodic boundary conditions were applied. The zeolite structure, including the cations, was considered as rigid. The effect of framework expansion upon loading and cation mobility have been studied experimentally by several authors.[2,3,5] In the case of faujasite NaY, the neutron diffraction study of Czjzek et al.[3] has revealed that the introduction of xylene into the cavities of the zeolite has only a small effect on the framework structure. The average T−O bond lengths and angles are hardly modified, and the sodium ion site occupancies do not change. On the contrary, Mellot et al.[5] have found that the adsorption of xylene in zeolite BaX can lead to a partial migration of cations from sites I and I′ to sites II. The influence of these effects, and especially the influence of the framework flexibility and the cation mobility upon the adsorption capacities and the shape of the simulated isotherms, will be studied in a future work.

TABLE 1: Partial Charges and Dipole Polarizabilities of Zeolite Species and Xylene atoms

NaY	O	Si, Al	Na
q (|e|)[33]	−0.823	+1.396	+1.0
α (Å^3)[a]	1.11	0.44	0.15
xylene	C_{ar}	H	CH_3
q (|e|)[34]	−0.115	+0.115	+0.115
α (Å^3)	1.90	0.64	2.00

[a] The dipole polarizabilities of zeolite species are only used for the calculation of the dispersion coefficients.

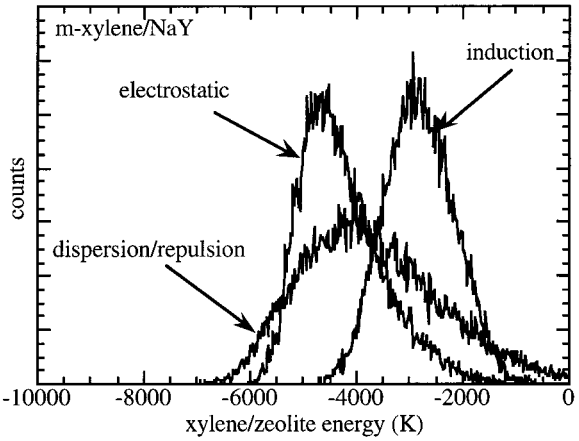

Figure 2. Electrostatic, dispersion/repulsion and induction contributions to the total *m*-xylene/NaY potential energy.

Interaction Potentials. The adsorbate−zeolite potential function used in this work considers the interactions between each atom of the adsorbate molecule with each zeolite species including Coulombic, induction, dispersion, and repulsion terms. The Coulombic energy is calculated using the Ewald sums technique. The partial charges[33,34] of all interacting species are given in Table 1. Figure 2 shows the histograms, averaged over 200 000 configurations, of the different contributions to the *m*-xylene/NaY potential energy. For this system, the electrostatic energy accounts for about 42%, the dispersion/repulsion term for about 33%, and the induction part for 25% of the total potential energy.

The dispersion energy is given by the following expression

$$U^{\text{disp}}(r_{ij}) = -\left(f_6 \frac{C_6^{ij}}{r_{ij}^6} + f_8 \frac{C_8^{ij}}{r_{ij}^8} + f_{10} \frac{C_{10}^{ij}}{r_{ij}^{10}}\right) \qquad (1)$$

with

$$f_{2n} = 1 - \sum_{k=0}^{2n} \frac{(b^{ij} r_{ij})^k}{k!} \mathrm{e}^{-b^{ij} r_{ij}}; \quad n = 3, 4, 5 \qquad (2)$$

Pellenq and Nicholson[35] have recently shown that the dispersion coefficients (C_6^{ij}, C_8^{ij}, C_{10}^{ij}, ...) can all be estimated from the knowledge of the dipole polarizabilities and the partial charges of all the interacting species. These dispersion coefficients are given in Table 2. The f_{2n} functions are damping functions used to represent possible electronic exchange between the two species in interaction. Their effect is to attenuate the dispersion part of the potential function at short distances.[36] These functions are parametrized with the single repulsive parameter b^{ij} corresponding to each interacting atomic pair.

TABLE 2: Dispersion Coefficients[a] Used for Absorbate−Zeolite Interactions

	O	T	Na
C_6 (Eh.a_0^6)			
C	41.99	16.97	7.36
H	12.83	5.18	2.19
CH_3	51.76	20.95	9.58
C_8 (Eh.a_0^8)			
C	948.54	341.97	125.78
H	226.45	78.73	28.08
CH_3	1111.09	399.88	149.53
C_{10} (Eh.a_0^{10})			
C	21725.50		2343.44
H	4153.60		395.97
CH_3	24685.35		2641.58

[a] In atomic units: 1 hartree (Eh) = 4.359814×10^{-18} J and 1 a_0 = 0.529177 Å.

TABLE 3: Repulsive Parameters Used for the Adsorbate−Zeolite Interaction

pair	A (10^8 K)	b (Å^{-1})
O−O	4.87	4.16
T−T		
Na−Na	1.46	3.78
C−C	0.45	3.61
H−H	0.29	5.48
CH_3−CH_3	1.08	3.36

The repulsion energy between atomic pairs is represented with an exponential Born−Mayer term

$$U^{\text{rep}}(r_{ij}) = A^{ij} \mathrm{e}^{-b^{ij} r^{ij}} \qquad (3)$$

The subscripts i and j stand for the atoms of the adsorbate molecule and the zeolite species, respectively. We have checked that the repulsive interaction between the adsorbate and T atoms (silicon or aluminum) can be neglected because the inner faces of a supercage cavity are covered with oxygen atoms and with sodium cations (the T atoms being further away in the crystal). We have used Böhm and Ahlrichs[37] combination rules to estimate the repulsive parameters A^{ij} and b^{ij} for a pair of heteroatoms ij using those of the ii and jj pairs

$$A^{ij} = (A^{ii} A^{jj})^{1/2}$$

$$\frac{2}{b^{ij}} = \frac{1}{b^{ii}} + \frac{1}{b^{jj}} \qquad (4)$$

The values of the repulsive parameters for each ii and jj pair are reported in Table 3. The oxygen/oxygen and sodium/sodium parameters were first estimated from values found in the literature[38,39] and then readjusted in order to reproduce the isosteric heat of adsorption at zero coverage. It is noteworthy that these parameters were only reajusted for one isomer (*m*-xylene) and the same values were then used for the other isomer. The carbon/carbon, hydrogen/hydrogen, and methyl/methyl repulsive parameters were obtained from the fit of the repulsive part of the short-range Lennard-Jones potential function used for the xylene/xylene interaction (see next section).

The calculation of the induction energy, U^{ind}, was performed using the first term of the multipole expansion only

$$U^{\text{ind}} = \sum_{i \in \text{ads}} -{}^1/_2 \alpha_i \vec{E}_{i0}{}^2 \qquad (5)$$

where α_i is the dipole polarizability of atom i of an adsorbed xylene molecule and $\vec{E}_{i0}$ is the electrostatic field at the position occupied by atom i due to the partial charges carried by all the

TABLE 4: Magnitude of the Different Contributions to the Adsorbate−Zeolite Interaction (K)

	dispersion					
electrostatic	C_6	C_8	C_{10}	repulsion	induction	back-polarization
−3030	−7218	−2086	−716	7875	−2136	139

framework species. This induction term contributes for about 25% to the total interaction energy (see Figure 2). Such a large contribution of the induction energy to the total adsorption energy is larger than what is usually expected. However, Pellenq et al.[27] have found that in the case of xenon atoms adsorbed in zeolite NaY the induction term amounts to 17% of the total Xe zeolite potential. In the case of xenon and argon adsorption in silicalite, the same author[35] has found that the induction contributes less than 0.3% of the total potential energy. These are interesting results since most models of adsorption in zeolites have ignored the induction term regardless of the zeolite nature. In the case of the cationic zeolite NaY, our calculations show that the electrostatic field is ∼7 *V*/nm at the adsorption site of a xylene molecule. The charges used for these calculations were −0.823 for O, 1.396 for Si/Al atoms, and 1.0 for Na.[33] Test calculations have been performed using another set of charges (−0.7 for O, 1.2 for Si/Al, and 0.8 for Na[40]) in order to check the effect of the partial charge values on the calculated electrostatic field. The electrostatic field calculated in this case at the adsorption sites is ∼6 V/nm, and the induction energy is 20% of the total adsorbate−zeolite potential. The values of the electrostatic field calculated with both sets of charges are within the range 5−18 V/nm of the available data[41,42] obtained from quantum mechanical calculations at a distance of ∼3.0 Å from the cations.

The contribution of back-polarization effects and higher order terms of the induction energy have been evaluated as follows in order to check the consistency of our potential functions.

The dipole moment $\vec{\mu}_i$ induced in a particle *i* is determined by its polarizability and the electrostatic field $\vec{E}_i$ due to external sources

$$\vec{\mu}_\iota = \alpha_i \vec{E}_i \tag{6}$$

Assuming that these external sources are the partial charges carried by the zeolite atoms only, the electrostatic field $\vec{E}_i$ is equal to $\vec{E}_{i0}$:

$$\vec{E}_{i0} = -\sum_{j\neq i}^{j\in \text{zeo}} q_j \frac{\vec{r}_{ij}}{r_{ij}^3} \tag{7}$$

If we now take into account both partial charges q_j and induced moments $\vec{\mu}_j$, the electrostatic field is

$$\vec{E}_i = \vec{E}_{i0} + \sum_{j\neq i}^{j\in \text{zeo,ads}} T_{ij}\vec{\mu}_j \tag{8}$$

Equation 8 defines $\vec{E}_i$ as the sum of the permanent field $\vec{E}_{i0}$ and the total field from the induced moments, both at position *i*. The matrix T_{ij} is the dipole field tensor

$$T_{ij} = \frac{3}{(r_{ij})^5}\begin{bmatrix} x^2 & xy & xz \\ yz & y^2 & yz \\ zx & zy & z^2 \end{bmatrix} - \frac{I}{(r_{ij})^3} \tag{9}$$

where *I* is the unit tensor and *x*, *y*, *z* are the Cartesian components of the vector connecting atoms *i* and *j*. For a given set of particle positions, eqs 6 and 8 provide linear relations which determine the field $\vec{E}_i$ and moments $\vec{\mu}_i$. The corresponding polarization energy is simply

$$U^{\text{ind}} = \sum_{i\in\text{ads}} -{}^1/_2 \alpha_i \vec{E}_i \vec{E}_{i0} \tag{10}$$

Figure 3 presents the induction energy of a *m*-xylene molecule in the zeolite cavity as a function of the number of iterations performed for the calculation of the field and the induced dipoles. The value corresponding to a number of iterations equal to zero is the induction energy without taking into account back-polarization effects. Only a few iterations (∼5) are needed to reach convergency. The back-polarization effect accounts, in our system, for about 6% of the total induction energy. Table 4 shows the magnitude of the different contributions to the adsorbate−zeolite interaction. These values are not averaged data but have been calculated for one molecule of *m*-xylene only adsorbed at a given position in the zeolite NaY close to a sodium cation. Averaged data can be found in Figure 2. The back-polarization effect is the smallest term and has been neglected here. The magnitudes of higher order terms in the developpement of the induction energy (eq 5), such as quadrupoles induced by the electrostatic field or dipoles and quadrupoles induced by the field gradient, and hyperpolarizabilities as well, have been estimated and were found to be quite low (less than 5% of the total induction energy).

It is important to stress that the adsorbate−zeolite potential function used in this work is easily transferable to any type of zeolite. It has been used successfully for different adsorbate−zeolite systems, such as argon and nitrogen in silicalite,[43] methane in $AlPO_4$-5,[38] and xenon, methane and xylene in different faujasites.[27] The use of this potential model, rather than a simple Lennard-Jones type potential, was found to be crucial in order to reproduce details of the adsorption properties, such as the substep in the isotherms of methane adsorbed in $AlPO_4$-5[38] and argon and nitrogen in silicalite.[40] The assumed rigidity of the adsorbent allowed us to calculate the external potential due to the faujasite at a large number of grid points in the pore prior to the simulations. The adsorbate−zeolite interaction potential during the runs was then calculated by linear interpolation. The number of grid points, reduced by the symmetry of the unit cell, was 262 701, leading to a grid spacing of less than 0.25 Å in each direction.

m-Xylene and *p*-xylene were assumed to be rigid, planar molecules, consisting of carbon atoms, hydrogen atoms, and methyl groups. Carbon−carbon, carbon−hydrogen, and carbon−methyl lengths were fixed at 1.40, 1.08, and 1.51 Å respectively. The carbon−carbon−carbon, carbon−carbon−hydrogen, and carbon−carbon−methyl angles were set to 120°. Xylene molecules were treated atom by atom except for methyl groups, which were taken as united atoms centered on the carbon atoms. The potential energy between two adsorbed molecules is the sum of a dispersion−repulsion term, modeled by a Lennard-Jones type potential, plus a Coulombic term

$$U_{ij} = -4\epsilon_{ij}\left[\left(\frac{\sigma_{ij}}{r_{ij}}\right)^6 - \left(\frac{\sigma_{ij}}{r_{ij}}\right)^{12}\right] + \frac{q_i q_j}{r_{ij}} \tag{11}$$

The Lennard-Jones parameters σ_{ii} and ϵ_{ii} used in this work (see Table 5) and the partial charges (see Table 1) are taken from

TABLE 5: Lennard-Jones Parameters for Xylene−Xylene Interaction

	σ (Å)	ϵ (K)
C−C	3.55	35.24
H−H	2.42	15.08
CH_3-CH_3	3.80	85.47

the optimized potentials for liquid simulations (OPLS) proposed by Jorgensen.[34] The cross terms, σ_{ij} and ϵ_{ij}, are obtained using the Lorentz−Berthelot combination rules.[44] The OPLS partial charge distribution along with the xylene molecule geometry yields a dipole moment of 0.24 D for *m*-xylene, which is somewhat lower than the experimental gas phase value of 0.36 D. No attempt was made here to readjust the OPLS charges in view of the fair representation of the bulk fluid properties observed using this force field.[34]

Biased Grand Canonical Monte Carlo Calculations. The Monte Carlo process is governed, at equilibrium, by the following detailed balance equation:

$$P_{\mathrm{o}}^{\mathrm{Boltz}} \cdot P_{\mathrm{o}\to\mathrm{n}}^{\mathrm{gen}} \cdot P_{\mathrm{o}\to\mathrm{n}}^{\mathrm{acc}} = P_{\mathrm{n}}^{\mathrm{Boltz}} \cdot P_{\mathrm{n}\to\mathrm{o}}^{\mathrm{gen}} \cdot P_{\mathrm{n}\to\mathrm{o}}^{\mathrm{acc}} \tag{12}$$

where P^{Boltz} is the Boltzmann probability of a microscopic state, subscripts "o" (for "old") and "n" (for "new") refer to configurations of the system before and after a move, respectively, and P^{gen} and P^{acc} are the probabilities to generate and to accept this move.

In a standard GCMC simulation, three types of moves are performed. The first consists of a displacement and/or rotation step, handled by the usual Metropolis method.[45] In the second type of move, a new molecule is inserted into the system (transferred from the gas to the zeolite) at a randomly chosen position with a randomly chosen orientation. In the third type of move, a molecule is randomly chosen and removed. For a two-component system, it is possible to use an additional type of trial (swap) which consists of changing the identities of adsorbed particles without changing their positions and orientations.[46]

When these Monte Carlo moves are randomly generated, the probabilities of generating a specified move is equal to the probability to generate the inverse move, and the acceptance probabilities only depend on the Boltzmann factor as follows:

$$P_{\mathrm{displacement/rotation}}^{\mathrm{acc}} = \min(1, \mathrm{e}^{-\beta(U_n - U_o)}) \tag{13}$$

$$P_{\mathrm{insertion}}^{\mathrm{acc}} = \min\left(1, \frac{z_i V}{N_i + 1} \mathrm{e}^{-\beta(U_n - U_o)}\right) \tag{14}$$

$$P_{\mathrm{deletion}}^{\mathrm{acc}} = \min\left(1, \frac{N_i}{z_i V} \mathrm{e}^{-\beta(U_n - U_o)}\right) \tag{15}$$

$$P_{\mathrm{swap}i\to j}^{\mathrm{acc}} = \min\left(1, \frac{z_j N_i}{(N_j + 12) z_i} \mathrm{e}^{-\beta(U_n - U_o)}\right) \tag{16}$$

The subscripts *i* and *j* refer to the two components in the case of a binary mixture. *N* is the number of molecules in the system before the MC move, *V* is the volume of the simulation box, $\beta = 1/kT$, where *k* is the Boltzmann constant and *T* is the temperature, U_n and U_o are the energies of the configuration after and before the move, respectively, and z_i is the absolute activity of molecule *i*.

GCMC simulations have proven to be successful in predicting adsorption thermodynamic quantities of a variety of simple sorbates (argon, methane,[38] ...) in zeolites. Attempts to apply the normal GCMC technique to larger sorbates (benzene, xylene,[47] chain molecules,[48] ...) are bound to be frustrated by low acceptance rates of the insertion and deletion steps. In our study of xylene isomers in faujasites, these rates fell under 10^{-3}% at high loading. Thus, in order to sample the grand canonical ensemble correctly, the use of biased insertions and deletions is necessary.

The first bias consisted in reducing the volume *V* in which insertions were attempted. In a standard GCMC, these insertions are attempted uniformly throughout the volume of a unit cell of NaY zeolite. However, much of this volume (sodalite cages, volume filled by atoms of the framework ...) is inaccessible to xylene molecules. The accessible volume, V_{acc}, has a complex shape. It has been estimated using an energetic criterion. The total volume *V* was discretized into elementary volumes. An adsorbate molecule was placed at the center of each elementary volume and the corresponding adsorbate−zeolite interaction was calculated. V_{acc} is defined as the union of all elementary volumes corresponding to an interaction energy lower than an arbitrary positive value (1000 K in this work). For nonspherical molecules such as xylenes, this energy was calculated using a fictitious one-center-of-force model placed at the molecule center of mass. The potential parameters of the smallest adorbate atom, i.e. the hydrogen atom, were attributed to this fictious center of force. This procedure slightly overestimates V_{acc} but includes all possible adsorption sites. Xylene molecules can indeed be adsorbed at a distance of the zeolite wall smaller than the mean size of the molecule because of strong orientation effect. In the case of xylenes in NaY, the volume of the simulation box (one unit cell) is $V = 15352$ Å^3 and the accessible volume has been reduced to $V_{\mathrm{acc}} = 6886$ Å^3. In order to ensure microscopic reversibility, the acceptance rules for insertions and deletions must be modified by replacing the volume *V* by V_{acc}.

The second bias is the cavity bias proposed by Mezei.[49] In this method, insertions are only attempted in regions of the accessible volume where empty cavities of radius $R \geq R_{\mathrm{c}}$ exist. Such cavities can accommodate a particle insertion. In the case of xylene molecules, $R_{\mathrm{c}} = 3.5$ Å, which corresponds to the nearest-neighbor distance in the xylene center of mass pair distribution function. In the acceptance probabilities, *V* must be replaced by the volume of the subspace which is formed by the union of all points corresponding to the centers of a cavity of radius $R \geq R_{\mathrm{c}}$. This volume was estimated during the simulation by evaluating $P_{\mathrm{c}}(N)$, the probability of finding a suitable cavity in a configuration of *N* molecules (*N* is the total number of molecules). The volume in the acceptance probabilities is then multiplied by the factor $P_{\mathrm{c}}(N)$.

The third bias used here was an orientational bias.[50] In the case of a particle insertion, the method consists of generating *k* trial orientations ($k = 10$ in our work), and choosing the new configuration "*n*" out of these *k* trials with an energetic criterion. The new configuration is then generated with probability

$$P_{\mathrm{gas}\to\mathrm{zeo,n}}^{\mathrm{gen}} = \frac{\mathrm{e}^{-\beta U_n}}{\sum_{m=1}^{k} \mathrm{e}^{-\beta U_m}} \tag{17}$$

In order to calculate the acceptance probability of this biased move, the probability of generating the inverse move must also be calculated using the same process (see eq 12). In the case of a particle insertion, the inverse move consists of transferring a molecule from the zeolite to the gas reservoir. The gas phase is assumed to be ideal in the low pressure domain with zero

interaction energy. Following eq 17, the probability of generating a specified orientation out of k trial orientations in the reservoir is simply

$$P_{\text{zeo}\rightarrow\text{gas}}^{\text{gen}} = 1/k \tag{18}$$

Following eq 12, the acceptance probability of a particle insertion must be corrected by the probability of generating the move (eqs 17 and 18). The same procedure was applied to the deletion move which consists of transferring a molecule from the zeolite to the gas phase. The probability of generating such a move is given by eq 18. The probability to realize the inverse move is the probability to generate a molecule into the zeolite with the orientation "*o*" of the molecule to be deleted. Thus, $k - 1$ trial orientations must be generated and the probability to generate the transfer of a molecule from the gas to the zeolite with a specific orientation "*o*" was calculated as follows:

$$P_{\text{gas}\rightarrow\text{zeo,o}}^{\text{gen}} = \frac{e^{-\beta U_o}}{e^{-\beta U_o} + \sum_{m=1}^{k-1} e^{-\beta U_m}} \tag{19}$$

In our GCMC simulations, we have combined the three types of bias described above. Therefore, the acceptance probabilities for a particle insertion is

$$P_{\text{insertion}}^{\text{acc}} = \min\left(1, \left[\frac{(V_{\text{acc}}\cdot P_c(N))z_i}{N_i + 1} e^{-\beta(U_n - U_o)}\right]\cdot\left[\frac{W_n}{e^{-\beta U_n}}\frac{1}{k}\right]\right) \tag{20}$$

with

$$W_n = \sum_{m=1}^{k} e^{-\beta U_m} \tag{21}$$

The term in the first bracket in eq 20 corresponds to the standard Boltzmann probability ratio (eq 14), where the volume was reduced because of the first two types of bias. The second term is the correction due to orientational bias. U_o is the energy of the configuration before the move, i.e. when the molecule is in the reservoir phase and thus $U_o = 0$. Equation 20 can be rewritten as follows:

$$P_{\text{insertion}}^{\text{acc}} = \min\left(1, \left[\frac{(V_{\text{acc}}\cdot P_c(N))z_i}{N_i + 1}\frac{W_n}{k}\right]\right) \tag{22}$$

Similarly, the acceptance probability of a particle deletion is

$$P_{\text{deletion}}^{\text{acc}} = \min\left(1, \left[\frac{N_i}{z_i(V_{\text{acc}}P_c(N-1))}\frac{k}{W_o}\right]\right) \tag{23}$$

with

$$W_o = e^{-\beta U_o} + \sum_{m=1}^{k-1} e^{-\beta U_m} \tag{24}$$

Finally, we have also introduced an orientational bias in the identity swap move. Since the aromatic ring planes have roughly the same orientation in adsorption sites for both isomers (perpendicular to the (1,1,1) axis), we have used an orientation bias which retains the aromatic ring orientation. The orientation of a xylene molecule with respect to the zeolite coordinate axes was specified by three Eulerian angles, ϕ, θ, and φ, and the desired rotations (retaining the aromatic ring orientation) can be easily achieved by modifying only the φ angle. This procedure is analogous to the orientational bias for particle insertion and deletion except that the k trial orientations are all in the same plane. The acceptance probability of the i for j swap is

$$P_{\text{swap } i\rightarrow j}^{\text{acc}} = \min\left(1, \left[\frac{z_j N_i}{z_i(N_j + 1)}\frac{W_n}{W_o}\right]\right) \tag{25}$$

W_n and W_o are calculated using eqs 21 and 24 for molecules of type j and i, respectively.

We first performed unbiased GCMC simulations. Such simulations were characterized by low acceptance rates of the particle insertions and deletions and the corresponding amount of adsorbed molecules was underestimated at high density. We have tested our biased algorithms with simulations at low loading (less than one xylene per supercage of faujasite). These calculations were performed to verify that the standard GCMC and biased GCMC lead to the same results and to compare the efficiency of the two methods. Simulations have been performed on the Fujitsu VPP500 computer of the Institut Français du Pétrole, in Rueil-Malmaison, France. The computer code was optimized for vectorization. The introduction of bias multiplies by a factor of 7 the acceptance rate and only doubles the computing time. Tests have also been performed at high loading (three molecules of xylene per supercage of faujasite). Without using any biased algorithm, the insertion/deletion acceptance rate is lower than 10^{-3}%. This rate was increased to 0.15% when using all types of bias described above. Even after more than 7×10^6 Monte Carlo steps using standard GCMC, the average number of molecules is significantly lower than the average value obtained after 400 000 steps using biased algorithms. Therefore, careful attention must be paid to convergence when performing GCMC simulations of such complex systems at very high densities. In order to validate the maximum of loading value, we constructed a test configuration with one molecule placed in each possible adsorption site. The localization of each individual molecule was then optimized using canonical Monte Carlo to obtain a realistic low potential energy configuration with a loading greater than the expected maximal loading. Two sets of grand canonical simulations were performed, starting from either this configuration or a lower density configuration. They both converged to the same maximal number of adsorbed molecules. This indicates that our biased algorithm allows to obtain the stable maximum of loading value for this system. In the case of mixture adsorption, the introduction of identity change moves was found to be crucial for convergence. More details about our biased algorithms can be found in ref 51.

III. Results and Discussion

Adsorption of Pure Components. The calculated adsorption isotherms of pure *m*-xylene and pure *p*-xylene in NaY at 423 K are shown in Figure 4. The simulated curves are compared to their experimental counterparts at the same temperature.[9] The GCMC simulations predict type I isotherms for both isomers in agreement with experiments.[9] As in experiments, no hysteresis was found when performing simulations by increasing the pressure, starting from empty cavities, or by decreasing the pressure, starting from filled cavities. The amount of adsorbed molecules is lower for *p*-xylene than for *m*-xylene over all the pressure range. The maximal loading is 3.31 molecules per supercage for *p*-xylene and 3.54 for *m*-xylene. These values can be compared to the experimental data of Bellat et al.[9] at the same temperature. They found an adsorption capacity of

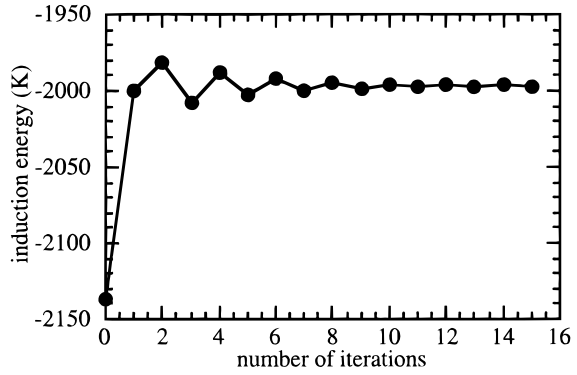

Figure 3. *m*-Xylene/NaY induction energy as a function of the number of iterations done for the calculation of back-polarization.

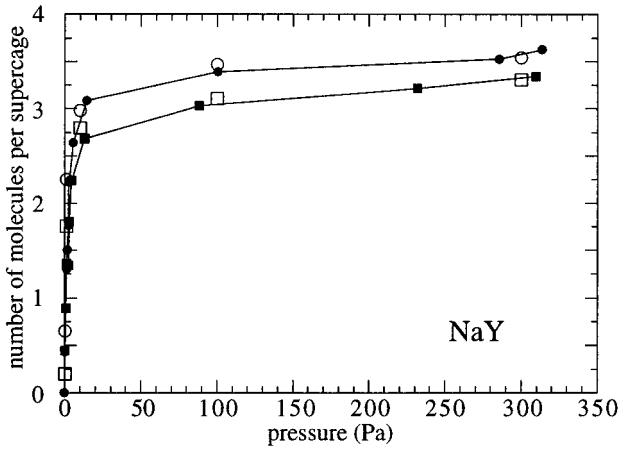

Figure 4. Simulated (open symbols) and experimental (filled symbols) adsorption isotherms at 423 K for pure *m*-xylene (circles) and pure *p*-xylene (squares) in the NaY zeolite.

3.3 *p*-xylenes per supercage and 3.6 *m*-xylenes per supercage. In the present work, the uncertainty on the average number of particles in the system is 0.25 molecule per supercage.

The isosteric heat of adsorption in zeolite NaY was calculated during the simulation using the usual expression

$$Q_{st} = RT - \frac{\langle NU\rangle - \langle N\rangle\langle U\rangle}{\langle N^2\rangle - \langle N\rangle^2} \qquad (26)$$

where $\langle\ \rangle$ refers to the average over the simulation run, N is the number of molecules, and U is the energy. This formula allows to compute separately the contributions to the isosteric from the adsorbate−adsorbate and adsorbate−zeolite interactions by either taking U as the total energy or the revelant component energies. Zero coverage data obtained from the simulation were compared to experiment in order to validate the xylene−zeolite potential function used in this work. The simulated zero coverage isosteric heat for *m*-xylene in NaY was equal to 97 ± 5 kJ/mol. The xylene potential parameters were adjusted, prior to the simulation, so that this value lies in the range of reported experimental data: 75 ± 6,[10] 84.5,[16] and 125 kJ/mol.[52] For *p*-xylene, the zero coverage isosteric heat of adsorption in NaY obtained from simulation is 82 ± 5 kJ/mol. This value also lies in the range of experimental data: 70 ± 6,[10] 76.5,[16] 114,[45] 89.3 kJ/mol.[53] Because of the discrepancy between these different experimental results, the comparison between simulated and measured zero coverage data cannot be used to validate the adsorbate−zeolite force field used in this work. In the case of simpler sorbates, such as xenon and methane, for which accurate experimental data are available, Henry constants and zero coverage heats of adsorption calculated using the same type of adsorbate−zeolite potential function were shown to be in good agreement with experiments. More details about this previous study can be found in reference.[27] Figure 5 shows the evolution of the isosteric heat of adsorption in NaY with coverage at 423 K. Its two separate contributions (adsorbate−zeolite and adsorbate−adsorbate) are also shown. The simulation results are compared with those obtained experimentally by Bellat et al.[10] The simulation reveals that the adsorbate−zeolite contribution to the isosteric heat of adsorption is nearly constant with loading, which means that all the xylene molecules are adsorbed on energetically identical sites. The *p*-xylene isosteric heat of adsorption is always lower than the one for *m*-xylene whatever the loading. The same behavior has also been observed experimentally by Bellat et al.[10] This difference between the two isomers is due to a smaller adsorbate−zeolite contribution in the case of *p*-xylene, whereas the adsorbate−adsorbate contribution is the same for both isomers.

Additional information can be obtained by examining the computed histograms of the adsorbate−zeolite potential experienced by individual molecules (see Figure 6). The average interaction energies with the NaY zeolite framework were found to be −11 300 K (−93.9 kJ/mol) and −10 000 K (−83.1 kJ/mol) for one molecule of *m*-xylene and *p*-xylene, respectively. These data are of the same order of magnitude as the recent values of Kitagawa et al.[28] obtained from canonical Monte Carlo simulations with a Lennard-Jones type potential. These authors reported values of −125 kJ/mol for *m*-xylene and −110 kJ/

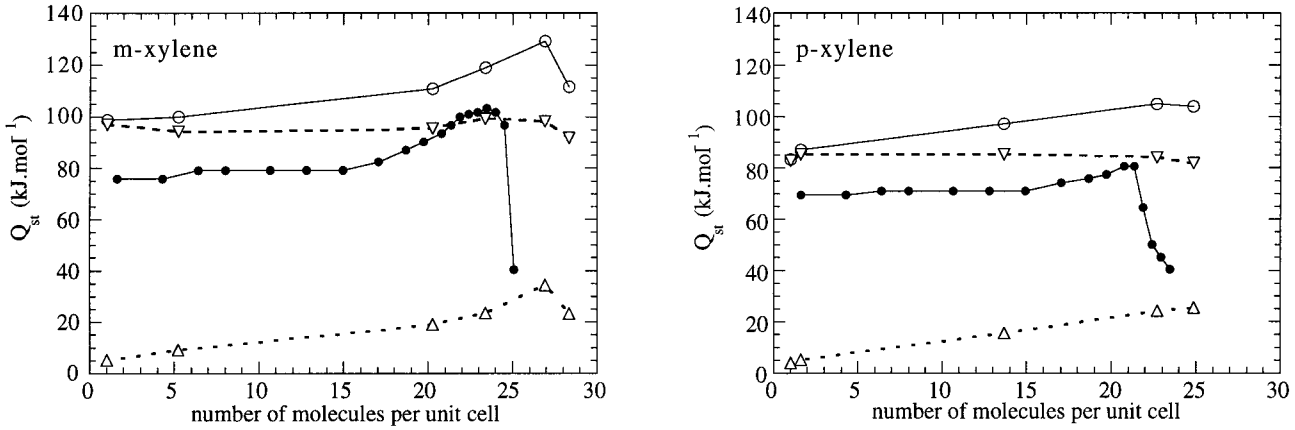

Figure 5. *m*-Xylene (left) and *p*-xylene (right) isosteric heat curve in NaY at 423 K. The adsorbate−adsorbate (open up triangle) and the adsorbate−zeolite (open down triangle) contributions to the total (simulated) heat curve (open circle) are shown. The total simulated curve is compared to the experimental curve[10] (filled circle).

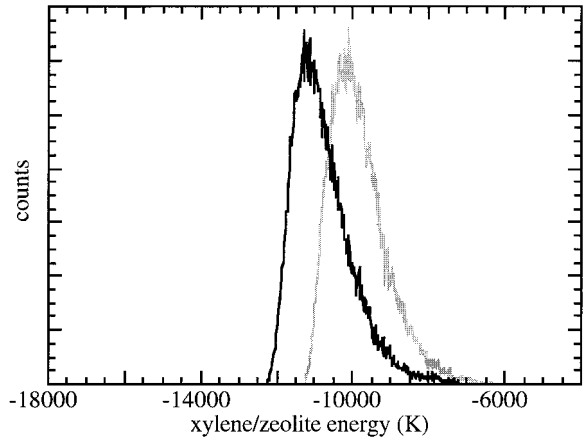

Figure 6. Xylene/zeolite potential energy distribution for *m*-xylene (black line) and *p*-xylene (gray line).

mol for *p*-xylene. The *m*-xylene−zeolite interaction is of ∼15 kJ/mol stronger than the *p*-xylene−zeolite one. The examination of the different contributions to the total xylene−zeolite interaction reveals that this difference between the two isomers is due to stronger electrotatic and induction interactions in the case of the *m*-xylene, whereas the dispersion energy is in favor of *p*-xylene. No significant change in the energy distribution is observed when increasing the pressure, meaning that xylene molecules lie in the same adsorption sites whatever the loading.

Location of Adsorbed Molecules. In order to characterize the location of the adsorbed molecules obtained from our simulations, several distances and angle histograms have been calculated. All these histograms are averaged over 200 000 configurations and were calculated from configurations at high loading ($P = 300$ Pa). The corresponding curves at low loading, not shown in this work, are very similar. No specific ordering has been observed when increasing the density. Both xylene isomers were found to be adsorbed in supercages in front of the sodium cations in site II. No molecule was ever observed in the circular 12-membered ring windows (see Figure 7b showing the distance between the xylene center of mass and the nearest window center). Figure 7a shows the sodium−xylene center of mass distance at high pressure ($P = 300$ Pa). The average sodium−*m*-xylene distance is 2.9 Å and the average sodium−*p*-xylene distance is 3.2 Å. This is in agreement with the neutron diffraction study of Czjzek et al.,[3] who have reported a decrease of the Na^+ ring center distance in going from *p*-xylene to *m*-xylene, which indicates a decrease of the Na^+−xylene interaction. This diffraction study also reveals that the plane of the aromatic ring of both isomers is perpendicular to the (1,1,1) axis and that the center of the ring lies on the axis. Figure 7, c and d shows histograms of the distance between the xylene center of mass and the (1,1,1) axis and the angle between the aromatic ring and the (1,1,1) axis. Centers of mass of adsorbed molecules are not perfectly localized on the (1,1,1) axis, and aromatic rings are not exactly perpendicular to this axis: the average distance to the axis is ∼0.5 Å and the average angle is ∼5°. A snapshot of a *m*-xylene molecule adsorbed in front of a site II sodium cation is shown in Figure 1b. The energy and geometry of this configuration are close to the average values reported on previous histograms.

Adsorption of Binary Mixtures. Simulations of coadsorption were carried out for binary mixtures of various gas phase compositions: an equimolar mixture, a mixture with 20% *p*-xylene and 80% *m*-xylene, and a mixture with 80% *m*-xylene

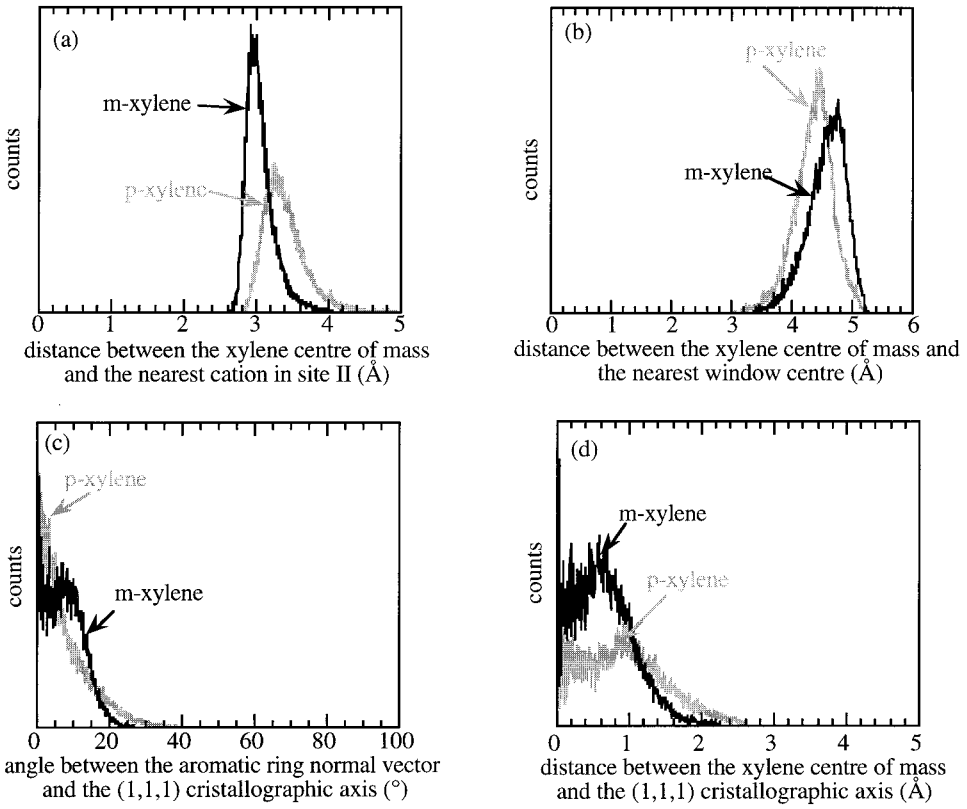

Figure 7. (a) Distribution of the distances between the xylene center of mass and the nearest cation in site II. (b) Distribution of the distances between the xylene center of mass and the nearest 12-ring window center. (c) Distribution of the angles between the (1,1,1) crystallographic axis and the aromatic ring normal vector of an adsorbed xylene. (d) Distribution of the distances to the (1,1,1) crystallographic axis of the xylene center of mass. All these histograms are averaged over 200 000 configurations at high loading (300 Pa). The black lines correspond to *m*-xylene and the gray lines to *p*-xylene.

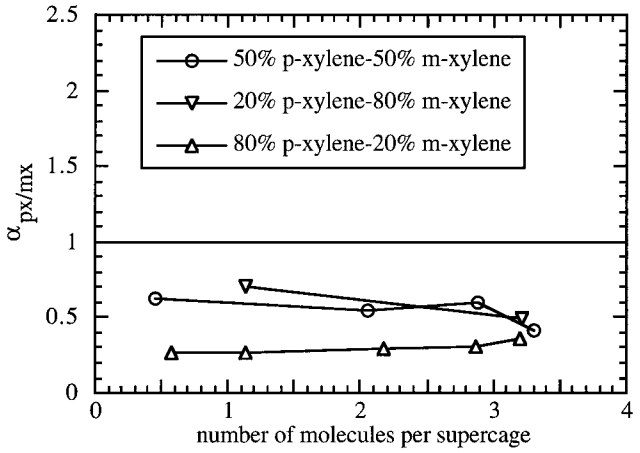

Figure 8. Variation of selectivity ($\alpha_{px/mx}$) with loading for *p*-xylene/*m*-xylene mixtures of various compositions.

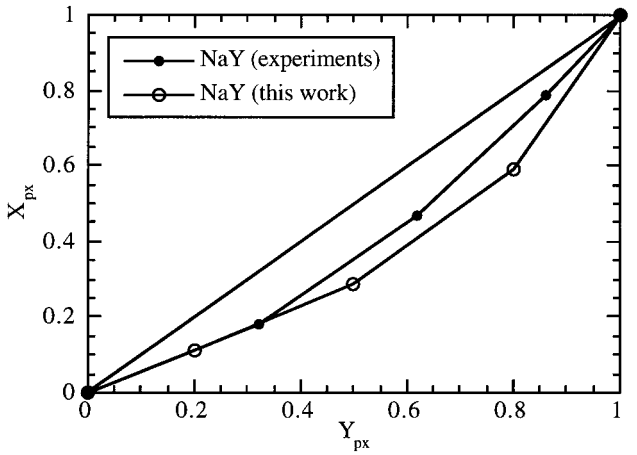

Figure 9. Molar fraction of *p*-xylene in the adsorbed phase (X_{px}) versus molar fraction of *p*-xylene in the gas-phase (Y_{px}) at high loading in zeolite NaY. The experimental curve[14,15] is also shown for comparison.

and 20% *p*-xylene. The adsorption selectivity for *p*-xylene was calculated using the equation

$$\alpha_{px/mx} = \frac{x_{px}}{x_{mx}} \frac{y_{mx}}{y_{px}} \tag{27}$$

where x_i and y_i are the molar fractions of component *i* in the adsorbed phase and in the gas phase, respectively. The selectivity as a function of the total amount of adsorbed molecules is shown in Figure 8 for the three mixtures.

Whatever the gas composition, the zeolite NaY appears to be selective for *m*-xylene ($\alpha_{px/mx} < 1$). This is in agreement with experimental results for equimolar mixtures at high loading of Cottier et al.[14,15] ($\alpha_{px/mx} = 0.5$) and of Iwayama et al.[22] ($\alpha_{px/mx} = 0.34$). No drastic change in the value of selectivity was observed as the total amount of adsorbed molecules increased. The same behavior has been observed experimentally[14,15] for a 20% *p*-xylene/80% *m*-xylene mixture ($\alpha_{px/mx} = 0.5$ whatever the number of adsorbed molecules). In the case of an equimolar mixture, experimentalists[14,15] have found no selectivity at low loading and a selectivity of 0.5 at high loading. This discrepancy might be due to our simulation model but we suggest that this may also be due to some kinetic effect in the experiments during the adsorption process. It is important to mention that the coadsorption results obtained from one mixture simulation cannot be directly compared to corresponding experimental data.[14,15] Indeed, during experimental measurements, the gas phase composition at equilibrium varies with the loading, whereas, in GCMC simulations of mixtures, the gas phase composition is constant (equal to the imposed value) whatever the pressure. Figure 9 shows the gas composition versus the adsorbed phase composition at high loading. The third simulated points correspond to the third studied mixtures (20% *p*-xylene/80% *m*-xylene, 50% *p*-xylene/50% *m*-xylene, and 80% *p*-xylene/20% *m*-xylene). Such diagrams can be directly compared to experiments.[14,15]

The various energy, distance, and angle histograms previously described for pure components have very similar shapes and the same position of maxima for mixtures. *m*- and *p*-xylene isomers exhibit the same behavior in both the single component and the binary mixture studies. Therefore, the selectivity cannot be explained in this case by a modification of the sorption properties of one isomer due to the presence of the other one. Single-component studies might have been sufficient for predicting the coadsorption selectivity of the xylenes/NaY system. No attempt was made here to use phenomenological models such as the ideal adsorption theory (IAS) to calculate the selectivity for a given mixture from the single species adsorption isotherms. However, direct coadsorption simulations or measurements are needed for the study of other faujasite selectivities, such as the barium Y faujasite for instance. For this system, the pure *m*-xylene and *p*-xylene isotherms are identical whereas BaY exhibits a selectivity in favor of *p*-xylene.[14,15]

IV. Conclusion

Molecular simulations of the adsorption and coadsorption of *m*-xylene and *p*-xylene in faujasite NaY were performed using a grand canonical ensemble Monte Carlo technique in which particle insertions and deletions were biased. These biased algorithms resulted in an improvement in the efficiency of the simulations compared to traditional GCMC, making it possible to study the adsorption of systems such as xylenes in faujasites at high loading that could not otherwise have been investigated with GCMC. The model used in this study was based on a detailed adsorbate−zeolite potential function combined with a simple zeolite structure; it is noteworthy that this model is fully transferable from one faujasite to the other. The simulated adsorption isotherms as well as the isosteric heat curves and the adsorption selectivities were systematically compared to available experimental data.

Results of the single-component study show, in agreement with experiments, that the adsorption capacities of the NaY zeolite is greater for *m*-xylene than for *p*-xylene. The adsorption selectivity predicted by the binary mixture study is in agreement with experiments. The structural analysis of the adsorbed phases has revealed a unique adsorption site in the supercages near the type II sodium counterions. GCMC studies of other xylene/faujasite systems are now in progress. The aim of these new works is to study the influence of the number of the extraframework cations and the influence of the nature of these cations upon the adsorption selectivity. Preliminary results obtained from the coadsorption of an equimolar mixture of xylene isomers in the NaX faujasite are very encouraging.[54] The absence of selectivity of this faujasite has been reproduced by our simulations using exactly the same potential model as in the case of NaY.

Acknowledgment. We thank the Institut Français du Pétrole for financial support through a BDI/CNRS grant for V.L. and for a generous allocation of FUJITSU computer time.

References and Notes

(1) Neuzil, R. W. U.S. Patent 3,558,730, 1971. Neuzil, R. W. U.S. Patent 3,558,732, 1971.

(2) Fitch, A. N.; Jobic, H.; Renouprez, A. *J. Phys. Chem.* **1986**, *90*, 1311.

(3) Czjzek, M.; Fuess, H.; Vogt, T. *J. Phys. Chem.* **1991**, *95*, 5255.

(4) Mellot, C.; Espinat, D.; Rebours, B.; Baerlocher, C.; Fischer, P. *Catal. Lett.* **1994**, 27, 159.

(5) Mellot, C.; Simonot-Grange, M.-H.; Pilverdier, E.; Bellat, J.-P.; Espinat, D. *Langmuir* **1995**, *11*, 1726.

(6) Descours, A. Ph.D. Thesis, Université de Bourgogne, 1997.

(7) Barthomeuf, D.; de Mallmann, A. *Ind. Eng. Chem. Res.* **1990**, *7*, 1437.

(8) Lian Su, B.; Manoli, J. M.; Potvin, C.; Barthomeuf, D. *J. Chem. Soc., Faraday Trans.* **1993**, 89, 857.

(9) Bellat, J.-P.; Simonot-Grange, M.-H.; Jullian, S. *Zeolites* **1995**, 15, 124.

(10) Bellat, J.-P.; Simonot-Grange, M.-H. *Zeolites* **1995**, 15, 219.

(11) Pilverdier, E. Ph.D. Thesis, Université de Bourgogne, 1995.

(12) Simonot-Grange, M.-H.; Bertrand, O.; Pilverdier, E.; Bellat, J.-P.; Paulin, C. *J. Therm. Anal* **1997**, 48, 741.

(13) Bellat, J.-P.; Pilverdier, E., Simonot-Grange, M.-H.; Jullian, S. *Microporous Mater*. **1997**, 9, 213.

(14) Cottier, V. Ph.D. Thesis, Université de Bourgogne, 1996.

(15) Cottier, V.; Bellat, J.-P.; Simonot-Grange, M.-H.; Méthivier, A. *J. Phys. Chem. B* **1997**, 101, 4798.

(16) Ruthven, D. M.; Goddard, M. V. *Zeolites* **1986**, 6, 275.

(17) Kärger, J.; Pfeifer, H. *Zeolites* **1989**, 9, 267.

(18) Kärger, J.; Ruthven, D. M. *Zeolites* **1987**, 7, 90.

(19) Eic, M.; Goddard, M. V.; Ruthven, D. M. *Zeolites* **1988**, 8, 258.

(20) Germanus, A.; Kärger, J.; Pfeifer, H.; Samulevic, N. N.; Zdanov, S. P. *Zeolites* **1985**, 5, 91.

(21) Jobic, H.; Bée, M.; Kärger, J.; Pfeifer, H.; Caro, J. *J. Chem. Soc., Chem. Commun.* **1990**, 341.

(22) Iwayama, K.; Suzuki, M. *Stud. Surf. Sci. Catal.* **1994**, 83, 5016.

(23) Santacesaria, E.; Morbidelli, M.; Danise, P.; Mercenari, M.; Carra, S. *Ind. Eng. Chem. Process Des. Dev.* **1982**, 21, 440.

(24) Hulme, R.; Rosensweig, R. E.; Ruthven, D. M. *Ind. Eng. Chem. Res.* **1991**, 30, 752.

(25) Bellat, J.-P.; Cottier, V.; Simonot-Grange, M.-H.; Allain, X.; Méthivier, A. *Récent Prog. Gén. Procédés* **1995**, 9, 159.

(26) Schrimpf, G.; Tavitian, B.; Espinat, D. *J. Phys. Chem.* **1995**, *99*, 10932.

(27) Pellenq, R. J−M.; Tavitian, B.; Espinat, D.; Fuchs, A. H. *Langmuir* **1996**, 12, 4768.

(28) Kitagawa, T.; Tsunekawa, T.; Iwayama, K. *Microporous Mater*. **1996**, 7, 227.

(29) Myers, A. L.; Prausnitz, J. M. *A.I.Ch.E.J*. **1965**, 9, 5.

(30) Mortier, W. J. *Compilation of Extra-Framework Sites in Zeolites*; Butterworth Scientific Ltd.: Guildford, U.K., 1982.

(31) Vitale, G.; Mellot, C. F., Bull, L. M.; Cheetham, A. K. *J. Phys. Chem. B* **1997**, 101, 4559.

(32) Eulenberger, G. R.; Shoemaker, D. P.; Keil, J. G. *J. Phys. Chem.* **1967**, *71*, 1812.

(33) Uytterhoeven, L.; Dompas, D.; Mortier, W. J. *J. Chem. Soc., Faraday Trans.* **1992**, 88, 2753.

(34) Jorgensen, W. L.; Nguyen, T. B. *J. Comput. Chem.* **1993**, 14, 195.

(35) Pellenq, R. J−M.; Nicholson, D. *J. Phys. Chem*. **1994**, 98, 13339.

(36) Tang, K.; Toennies, J. *J. Chem. Phys.* **1984**, 80, 3726.

(37) Böhm, H.; Ahlrichs, R. *J. Chem. Phys.* **1982**, 77, 5068.

(38) Lachet, V.; Boutin, A.; Pellenq, R. J−M.; Nicholson, D.; Fuchs, A. H. *J. Phys. Chem.* **1996**, *100*, 9006.

(39) Freitag, A.; van Wullen, C.; Staemmler, V. *Chem. Phys. Lett*. **1995**, 192, 267.

(40) Demontis, P.; Yashonath, S.; Klein, M. L. *J. Phys. Chem.* **1989**, *93*, 5016.

(41) Goursot, A.; Vasilyev, V.; Arbuznikov, A. *J. Phys. Chem.* B **1997**, 101, 6420.

(42) Angyan, J. G.; Ferenczy, G.; Nagy, P.; Naray-Szabo, G. *Collect. Czech. Chem. Commun.* **1988**, 53, 2308.

(43) Douguet, D.; Pellenq, R. J−M.; Boutin, A.; Fuchs, A. H.; Nicholson, D. *Mol. Sim.* **1996**, 17, 255.

(44) Allen, M. P.; Tildesley, D. *Computer Simulation of Liquids*; Clarendon Press: Oxford, U.K. 1987.

(45) Metropolis, N.; Rosenbluth, A. W.; Rosenbluth, M. N.; Teller, A. H. *J. Chem. Phys.* **1953**, 21, 1087.

(46) Cracknell, R.; Nicholson, D.; Quirke, N. *Mol. Phys.* **1993**, 80, 885.

(47) Snurr, Q.; Bell, A. T.; Theodorou, D. N. *J. Phys. Chem.* **1993**, *97*, 13742.

(48) Smit, B. *Mol. Phys.* **1995**, 85, 153.

(49) Mezei, M. *Mol. Phys.* **1980**, 40, 901.

(50) Frenkel, D.; Smit, B. *Understanding Molecular Simulation*; Academic Press: New York, 1996.

(51) Lachet, V.; Boutin, A.; Tavitian, B.; Fuchs, A. H. *Faraday Discuss.* **1997**, 106, 307.

(52) Santacesaria, E.; Geloso, D.; Danise, P.; Carra, S. *Ind. Eng. Chem. Process Des. Dev.* **1985**, 24, 78.

(53) Gorkey, Y. Ph.D. Thesis, University of New Brunswick, Fredericton, 1985.

(54) Lachet, V.; Boutin, A.; Tavitian, B.; Fuchs, A. H., manuscript in preparation.